ACS APPLIED MATERIALS & INTERFACES

Applications of Polymer, Composite, and Coating Materials

Dual-Emitting Eu(III)-Cu(II) Heterometallic-Organic Framework: Simultaneous, Selective and Sensitive Detection of Hydrogen Sulfide and Ascorbic Acid in a Wide Range

Xubin Zheng, Ruiqing Fan, Yang Song, Kai Xing, Ping Wang, and Yulin Yang

ACS Appl. Mater. Interfaces, **Just Accepted Manuscript** • DOI: 10.1021/acsami.8b11367 • Publication Date (Web): 31 Aug 2018

ACS Publications

is published by the American Chemical Society. 1155 Sixteenth Street N.W., Washington, DC 20036

Dual-Emitting Eu(III)-Cu(II) Heterometallic-Organic Framework: Simultaneous, Selective and Sensitive Detection of Hydrogen Sulfide and Ascorbic Acid in a Wide Range

Xubin Zheng,[†] Ruiqing Fan,*[,†] Yang Song,[†] Kai Xing,[†] Ping Wang[†] and Yulin Yang*[,†]

[†] MIIT Key Laboratory of Critical Materials Technology for New Energy Conversion and Storage, School of Chemistry and Chemical Engineering, Harbin Institute of Technology, P. R. China

* Corresponding Author: Ruiqing Fan and Yulin Yang
E-mail: fanruiqing@hit.edu.cn and ylyang@hit.edu.cn

ABSTRACT： As the important biomolecules, the deficiency or maladjustment of hydrogen sulfide (H_2S) or ascorbic acid (AA) is associated with the symptoms of the same diseases (e.g., cardiovascular disease or cancer). There is an urgent need to develop a fluorescent probe capable of distinguishing between H_2S and AA simultaneously. Here, we report the syntheses, structure, and property of the first dual-detection fluorescent probe which can differentiate H_2S or/and AA in aqueous media. Accordingly, a novel $[EuCu(pydc)_2(ox)_{0.5}(H_2O)_3 \cdot 1.5H_2O]_{2n}$ (**1**, H_2pydc = 2,3-pyridinedicarboxylic acid, ox = oxalic acid) for selective and sensitive detection of H_2S and AA in a wide range has been constructed (H_2S: [130 nM, +∞); AA: [55 nM, +∞)), exhibiting excellent catalytic activity comparable to horseradish peroxidase (HRP). And the highly efficient detection in human serum sample also proves the potential application in medical diagnosis. Meanwhile, an combinatorial logic gate (AND(INH)–OR) based on the activated **1** has also been constructed. Furthermore, this approach for simultaneous H_2S and AA detection suggests that the current work will expand the potential application of MOFs for dual or multiple detections in biomedical fields.

KEYWORDS: *metal-organic framework, bimetallic biosensor, catalysis, hydrogen sulfide, ascorbic acid, in a wide range*

■ INTRODUCTION

Reactive sulfur species (RSS), such as H_2S and bio-thiols, have formed an increasing research field because of the important physiological function.[1-3] Among these, hydrogen sulfide (H_2S) is probably the most attractive as it has been confirmed as the third gaseous transmitter following CO and NO.[4-6] It can regulate the state of intracellular redox and basic signalling processes, including neurotransmission, myocardial contractility, regulation of vascular tone, and insulin secretion.[7] Abnormal H_2S levels were identified to be related to Alzheimer's disease,[8] liver cirrhosis,[9] arterial hypertension[10] and cancer,[11] making it a potential target to diagnostics and treatment of these diseases. Meanwhile, ascorbic acid (AA), as a biological cofactor, is essential to human health and plays a vital role in many physiological and chemical processes.[12] The maladjustment of AA is also associated with the symptom of many diseases, such as scurvy, cardiovascular disease or cancer.[13] Then there is a serious challenge for the rapid diagnosis of disease because of the similar symptom related to H_2S or/and AA. Consequently, it is very meaningful to find a method that shows highly sensitive and selective detection of H_2S and AA. To date, such dual-detection probe for H_2S and AA has not been reported.

With the increasing knowledge available for sensing H_2S and AA,[13-23] It is now possible to develop a dual-detection fluorescent probe for differentiating between H_2S and AA. Such probe will be of great significance in understanding the physiological interaction between H_2S and AA. Although a simple mix of two specific probes can detect two analytes with different fluorescence signals, it is also hard to overcome the difficulties such as potential reaction, uneven loading and unknown interference between the two probes in one system. In addition, this strategy is further limited in cell or/and *in vivo* imaging because of the larger invasive effects, and possible different localization and metabolisms of the probe.[24-27] Therefore, it is significant (but also challenging) to design a single fluorescent probe that can easily distinguish between H_2S and AA. As shown in Scheme 1, we envisaged that the single fluorescent probe will contain two different and separate reaction sites A and B. In the

ideal case, each reactive site was designed to only react with one species (H_2S or AA) to cause the corresponding fluorescence response. To achieve this design, lanthanide-transition (4f-3d) heterometallic-organic frameworks,[28-30] combining the merits of transition-MOFs[31-33] (*e.g.*, excellent optical, electrical and catalytic property) and lanthanide-MOFs[33-35] (*e.g.*, sharp emission, large Stokes shift (>200 nm), relatively long excited-state fluorescence lifetime and high color purity), may be regarded as very suitable choice,[36] where two separate metal sites serve as reactive site for selective detection of H_2S and AA, respectively. However, the study of 4f-3d MOFs is still insufficient. It remains a challenge to select and design suitable building unit and assemble them into the 4f-3d MOFs with predictive structure and function because of the competitive reaction between two different types of metal ions with organic ligand.

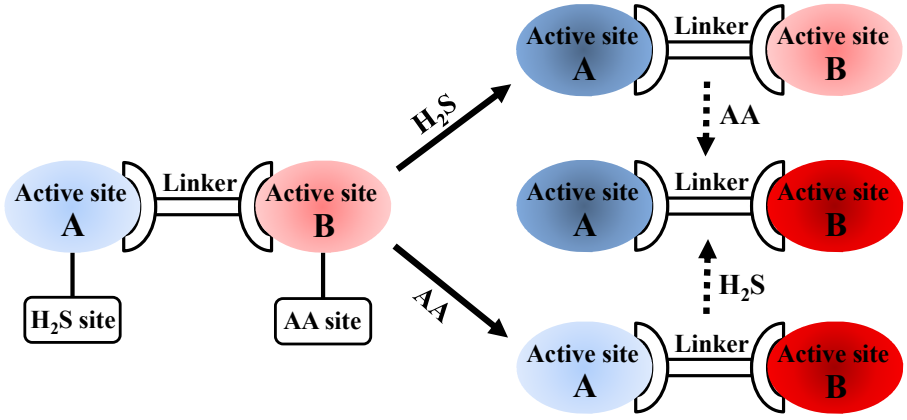

Scheme 1 The design of a single fluorescent probe for H_2S and AA detection.

Here, we report the rational design, synthesis, and evaluation of the first probe capable of distinguishing between H_2S and AA in bio-mimic environment and real sample. According to the design (Scheme 1), we have successfully synthesized one novel $[EuCu(pydc)_2(ox)_{0.5}(H_2O)_3 \cdot 1.5H_2O]_{2n}$ (**1**, H_2pydc = 2,3-pyridinedicarboxylic acid, ox = oxalic acid) for the first time. We envisaged that the size of the channel (10.1×14.6 $Å^2$) in **1**, which are larger than the maximize size of AA (7.0 Å) and H_2S (2.0 Å), could allow analytes to diffuse and react easily. Meanwhile, **1** also exhibits excellent stability towards water and simulated biological system, which is highly desirable for practical applications. As designed, the activated **1** (named as **1a** after)

shows selective and sensitive detection of H_2S or/and AA in a wide range (H_2S: [130 nM, +∞); AA: [55 nM, +∞)) and has been successfully applied to detect H_2S and AA in human serum samples. At the same time, **1a** is also found to exhibit excellent peroxidase-like activity and can catalyze the decomposition of H_2O_2 into ·OH, which plays a crucial role in the detection of AA and selective detection between H_2S and AA.

■ RESULTS AND DISCUSSION

Synthesis and characterization of 1

1 was obtained as blue crystal from the reaction of $Eu(NO_3)_3·6H_2O$, $Cu(NO_3)_2·3H_2O$, H_2pydc, and $Na_2C_2O_4$ by a hydrothermal method. Single crystal X-ray diffraction demonstrated that **1** crystallized in the monoclinic, space group *C* 2/c (Table S1, Supporting Information), with one tetra-coordinated Cu^{2+} ion, one octa-coordinated Eu^{3+} ion, two $pydc^{2-}$ ligands, half ox^{2-} bridge and three coordinated H_2O molecules per asymmetric unit (Figure S1, Supporting Information). Using Addison's model,[37] the coordination geometry of Cu^{2+} ion ($\tau_4 = 0.075$) could be better described as planar quadrilateral. As illustrated in Figure 1, the adjacent Eu^{3+} ions are bridged by ox^{2-} linker to form a secondary building unit [$Eu_2(C_2O_4)$]. Then the binuclear units are connected *via* $pydc^{2-}$ ligands with Cu^{2+} ions into 2D layer along the *a*-axis, which are further stitched to each other *via* π···π stacking interactions (Figure S2, Supporting Information), constructing a 3D heteromatellic-organic framework (Figure 1). The 3D framework exhibits 1D channels with the window size of approximately 10.1×14.6 $Å^2$. The PXRD pattern confirmed the crystalline purity (Figure S3a, Supporting Information).

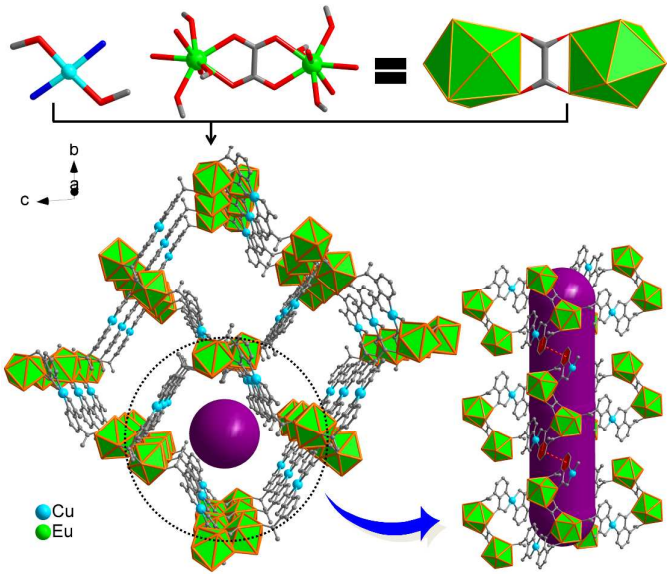

Figure 1. Crystal structure of **1** viewed along *a* crystallographic direction, showing coordination environments around Cu^{2+} and Eu^{3+}.

The structural stability of **1** to water environment is essential to meet the practical application. As demonstrated by PXRD, excellent water stability was observed when soaking the fresh sample of **1** in water for one week (Figure S3a, Supporting Information). At the same time, the PXRD patterns were still consistent with the simulated one when **1** was immersed in aqueous solution of pH value 3-8 for one day, indicating that **1** can be stably present in biological systems (Figure S3b, Supporting Information). Thermogravimetric experiment was also constructed to study the thermal stability of **1**. As shown in Figure S4 (Supporting Information), it gradually decreased about 12.30% up to 250 ^{o}C, which was assigned to the loss of free water and coordinated water (calculated: 12.18%). The free and coordinated water incorporated in **1** can be removed by pumping it under vacuum at 180 ^{o}C for 10 h, and the detailed structure of the activated sample **1a** was shown in Figure S5 (Supporting Information). Furthermore, the water-freed sample **1**a was verified by TGA, which showed similar thermal stability with fresh sample. The PXRD pattern of **1a** also confirmed the stability after water removal (Figure S3a, Supporting Information). But the SEM images of **1a** revealed the generation of the cracks on the surface after heat treatment (Figure S6a and S6b, Supporting Information).

As depicted in Figure S7 (Supporting Information), luminescence properties of **1**,

1a and H_2pydc were examined. The emission spectra of H_2pydc excited at 400 nm shows the maximum emission peak at 440 nm. Upon excitation of 315 nm (the excitation spectra was shown in Figure S7d, Supporting Information), the activated **1a** showed very similar emission spectrum to **1**. It is noteworthy that there were two luminescent centers in **1a**, which were attributed to the emission of Eu^{3+} ions and $pydc^{2-}$ ligands, respectively. The fluorescence peaks at 590, 615, 650, and 695 nm could be assigned to the $^5D_0 \rightarrow {}^7F_J$ (J = 1–4) transitions of the Eu^{3+} ions. However, the maximum emission at 365 nm, corresponding to $pydc^{2-}$ ligand, is much weaker than that of free H_2pydc ligand. Because of the unsaturated electronic state ($3d^9$), Cu^{2+} has a tendency to gain electrons. It will further promote the interaction between Cu^{2+} ions and Lewis basic carboxylic oxygen through the cooperative effect in the form of O–Cu–O,[38] which will increase the ligand-to-copper(II) charge transfer and reduce the ligand-to-europium(III) charge transfer, and then has no conducive to the emission of Eu^{3+} ions ((Figure S8, Supporting Information).

Hydrogen sulfide (H_2S) sensing

With the open metal site and unsaturated electronic state ($3d^9$), Cu^{2+} ion can react easily with guest of strong electron donor (*e.g.*, H_2S and thiol). Given the strong binding affinity of sulfide to Cu^{2+} ion, we explored the potential utility of **1a** as a turn-on sensor for H_2S detection. As expected, the emission of **1a** was immediately enhanced up to 9-fold after the addition of H_2S (Figure S9, Supporting Information). Subsequently, response time of **1a** to H_2S was investigated. The emission of **1a** rapidly increased and stabilized after 2 min (Figure S10, Supporting Information), which was faster than most reported H_2S probes. Next, the fluorescence responses of **1a** toward different concentrations of H_2S were also investigated to evaluate whether the developed sensor can be applied to quantitative detection of H_2S. As depicted in Figure 2, the emission intensity at 615 nm dramatically increased when the concentrations of H_2S ranged from 10 to 600 μM, and also showed a good linear relationship between the fluorescence intensity ratio (I_{615}/I_{365}-1) and the concentrations of H_2S (R^2=0.9924). Detection limit was determined as 130 nM ((LOD = 3δ/S) (Table S3, Supporting Information), which was lower than those previously

reported fluorescent sensors (Table S4, Supporting Information).[18-20, 38-40] These data indicated that **1a** can be used as an excellent sensor for H_2S.

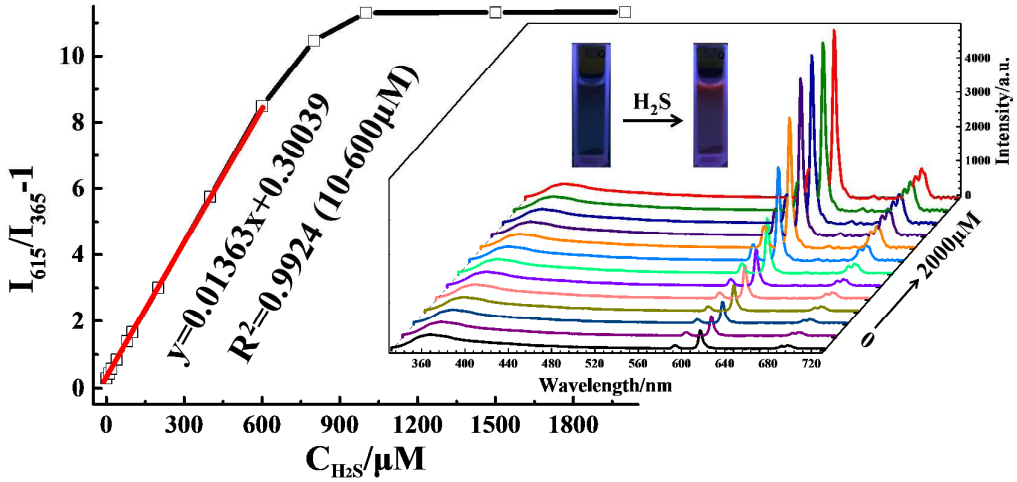

Figure 2. Concentration dependence and fluorescence spectra of **1a** with the increasing concentrations (0–2000 μM) of H_2S (λ_{ex} = 315 nm). Inset: Color photograph of **1a** in the presence of H_2S under 365 nm UV lamp

To illustrate the mechanism of H_2S sensing, PXRD spectra was performed. There was neither appearance of new band nor disappearance of the existing band before and after the addition of H_2S (Figure S11, Supporting Information). It could also be seen that the initial size and morphology of H_2S-treated **1a** did not change compared to original sample **1a** (Figure S6c and S6d, Supporting Information). Elemental analyses indicated an increase in the S content (Table S5, Supporting Information). The disappearance of the absorption peak of H_2S at 230 nm in the UV-Vis spectra also proves that H_2S can be absorbed into the framework (Figure S12, Supporting Information). X-ray photoelectron spectroscopy revealed a conspicuous shift of Cu $2p_{3/2}$ peak toward lower energy when treated with H_2S (from 932.8 to 932.2 eV) (Figure S13, Supporting Information), which is consistent with the mechanism by which H_2S acts as a strong electron donor to reduce the binding energy of the metal center.[41] These results confirmed that the interaction between H_2S and **1a** could result in the enhancement phenomenon, but it was not strong enough to destroy the crystalline structure of **1a**. Therefore, the following mechanism could be speculated: H_2S, as a strong electron donor, can reduce the interaction between Cu^{2+} ion and the $pydc^{2-}$ ligand by decreasing the binding energy of the metal center; as a result, to

reduce the ligand-to-copper(II) charge transfer and increase the ligand-to-europium(III) charge transfer ((Figure S8, Supporting Information)).

Catalysis of 1a for the reaction of H_2O_2 and AA

The catalytic activity of **1a** was investigated by the strong luminescence of the complex of Eu^{3+} ions and oxidized AA.[42] AA itself is colorless, and also cannot bond with Eu^{3+} ions to emit strong fluorescence even in the presence of H_2O_2 (Figure S14, Supporting Information). After the introduction of Cu^{2+} ion, the solution, containing Eu^{3+}, H_2O_2 and AA, became weakly fluorescent, showing that Cu^{2+} ion had a certain catalytic activity for the reaction of H_2O_2 and AA. However, upon the simultaneous addition of AA and H_2O_2, the luminescence intensity of **1a** at 615 nm was immediately enhanced up to 13-fold, which indicates that **1a** had significant catalytic activity to produce a large amount of oxidized AA. Obviously, the catalysis of **1a** is much better than that of Cu^{2+} ion, probably attributed to ligand environment and high porosity. To confirm the process of the reaction of AA and H_2O_2, we tested UV–visible spectra (Figure S15, Supporting Information). It is clear that the absorption peak of AA at 263 nm disappeared in the presence of H_2O_2 and **1a**, indicating the production of diketohexanoic acid (DA), which could be bond with Eu^{3+} ions and further result absence of UV-Vis absorption at 263 nm. In order to analyze the catalytic mechanism of **1a**, we also studied the fluorescence responses of p-phthalic acid (PTA) in the presence of H_2O_2 and **1a** (Figure S16, Supporting Information).[43] As a highly selective fluorescent probe for ·OH, PTA itself is non-fluorescence, but it could be combined with ·OH easily to produce 2-hydroxyterephthalic acid with highly fluorescent. The fluorescence of PTA was turned on upon the introduction of H_2O_2 and **1a** and gradually enhanced with increased concentrations of H_2O_2. These results indicate that H_2O_2 can be decomposed into ·OH in presence of **1a**, exhibiting high peroxidase-like catalytic ability, and the generated ·OH can react with AA to convert it into DA (Equation 1 and 2).

$$H_2O_2 \xrightarrow{\text{Eu(III)-Cu(II)-MOF}} 2\cdot OH \quad (1)$$

$$AA(C_6H_8O_6) + 2\cdot OH \rightarrow DA(C_6H_6O_6) + 2H_2O \quad (2)$$

The PXRD patterns and SEM images of AA/H_2O_2-treated **1a** confirmed the stability

(Figure S6e and S6f, Supporting Information).

Catalytic activity of **1a** as a peroxidase mimic was further investigated by the mean of steady-state kinetic experiment. As shown in Figure 3, it is obvious that Michaelis–Menten equation can be applied to the decomposition reaction catalyzed by **1a,** and K_m and V_{max} value can be directly calculated from Lineweaver–Burk plot. By definition, the smaller K_m value represents the stronger affinity of the enzyme to substrate. Consequently, the K_m value for **1a** to the catalytic reaction was determined as 3.0 mM, which is lower than that for the most-used horseradish peroxidase (HRP) (3.7 mM),[44-46] suggesting that **1a** has a stronger affinity and the requirement of **1a** for the concentration of H_2O_2 is lower when reached the maximum activity (Table S6, Supporting Information).

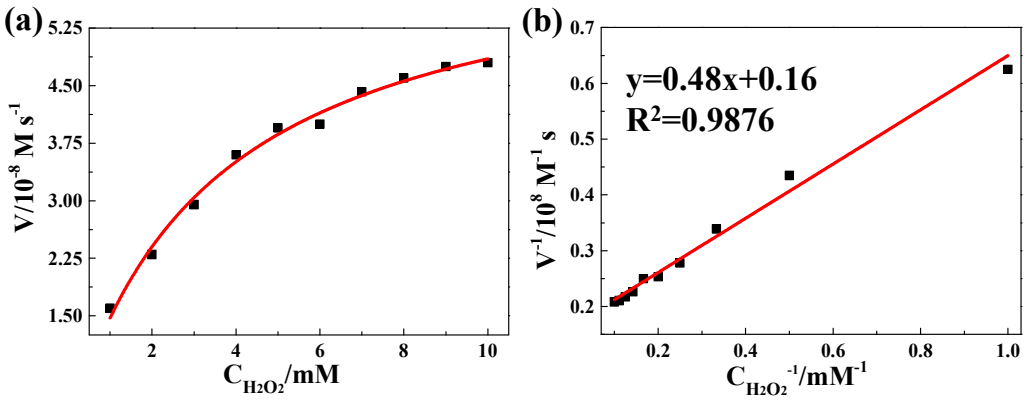

Figure 3. Steady-state kinetic assays of the **1a**, (a) Relationship between reaction rate and the concentration of H_2O_2 for the decomposition reaction catalyzed by **1a**, (b) Corresponding Lineweaver–Burk plot

Ascorbic acid (AA) sensing

Since the fluorescence intensity of **1a** is highly dependent on oxidized AA (DA), the method could be used as turn-on probe to quantitatively determine AA concentration in the presence of H_2O_2. Time-dependent luminescent spectra of AA/H_2O_2-treated **1a** revealed that the reaction of AA and H_2O_2 could be completed with 3 minutes (Figure S17, Supporting Information). The fluorescence responses of **1a** were further investigated with different concentrations of AA in the presence of H_2O_2 (Figure 4). Upon the gradual addition of AA, the fluorescence intensity of **1a** at 615 nm increased significantly with the concentration ranging from 10 μM to 400 μM,

whereas when the concentration exceeded 600 μM, there was only a slight increase. The linear relationship between I_{615}/I_{365}-1 and AA concentration (10−400 μM) (R^2=0.9972) indicated that **1a** can be used to quantitative detection of AA in the presence of H_2O_2. The detection limit for AA was calculated to 55 nM (Table S3, Supporting Information), which is similar to that of other probe based on fluorescent materials (Table S7, Supporting Information).[13, 21, 47-50]

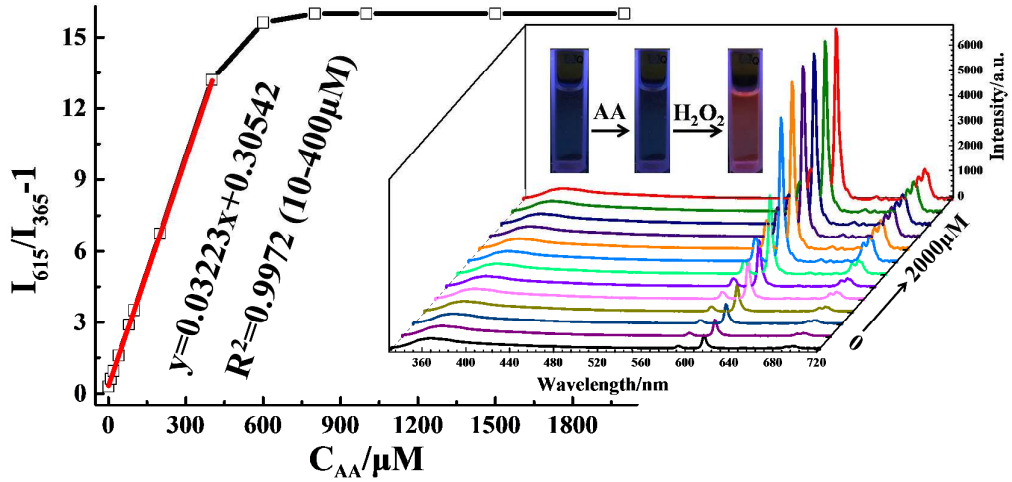

Figure 4. Concentration dependence and fluorescence spectra of **1a** with the increasing concentrations (0–2000 μM) of AA in the presence of H_2O_2 (5 mM) with λ_{ex} = 315 nm. Inset: Color photograph of **1a** in the presence of AA and H_2O_2 under 365 nm UV lamp

Selective detection between hydrogen sulfide (H_2S) and ascorbic acid (AA)

As an excellent biosensor, high selectivity is also quite crucial. To verify the selectivity of **1a**, fluorescence responses of **1a** toward 24 analytes were tested (Na^+, K^+, Ca^{2+}, Zn^{2+}, Fe^{2+}, I^-, Br^-, Cl^-, F^-, CH_3COO^-, $HCOO^-$, NO_3^-, NO_2^-, SO_3^{2-}, SO_4^{2-}, $S_2O_3^{2-}$, HCO_3^-, CO_3^{2-}, HPO_4^{2-}, PO_4^{3-}, GSH, Hcy, Cys and H_2S_2), which are related with the environment and organisms, in bio-mimic environment. Similar fluorescence responses of **1a** toward H_2S or H_2S_2 were observed under the same conditions (Figure S18, Supporting Information), indicating that the proposed probe **1a** cannot distinguish between H_2S and H_2S_2. But considering H_2S is a much more stable species than H_2S_2 and the endogenous H_2S concentration may be much higher than H_2S_2 in biological systems,[18] we adjusted the concentration of H_2S_2 to 0.1 mM for selective experiment. As shown in Figure 5, the fluorescent sensor of **1a** show almost negligible fluorescence to relevant analytes in the absence or presence of H_2O_2.

$S_2O_3^{2-}$ and the thiol-containing analytes (GSH, Hcy and Cys) had some effect on the fluorescence intensity of **1a** in the absence of H_2O_2 but showed no bearing on H_2S detection. More importantly, the addition of H_2S induced major increase of fluorescence intensity in the absence of H_2O_2 and restored to original state after the introduction of H_2O_2 (Figure 5b). Besides, the non-fluorescent AA was oxidized to generate DA to efficiently sensitize **1a** to emit strong fluorescence. These indicated that **1a** can act as a highly selective fluorescent probe for distinguishing between H_2S and AA *via* the introduction of H_2O_2.

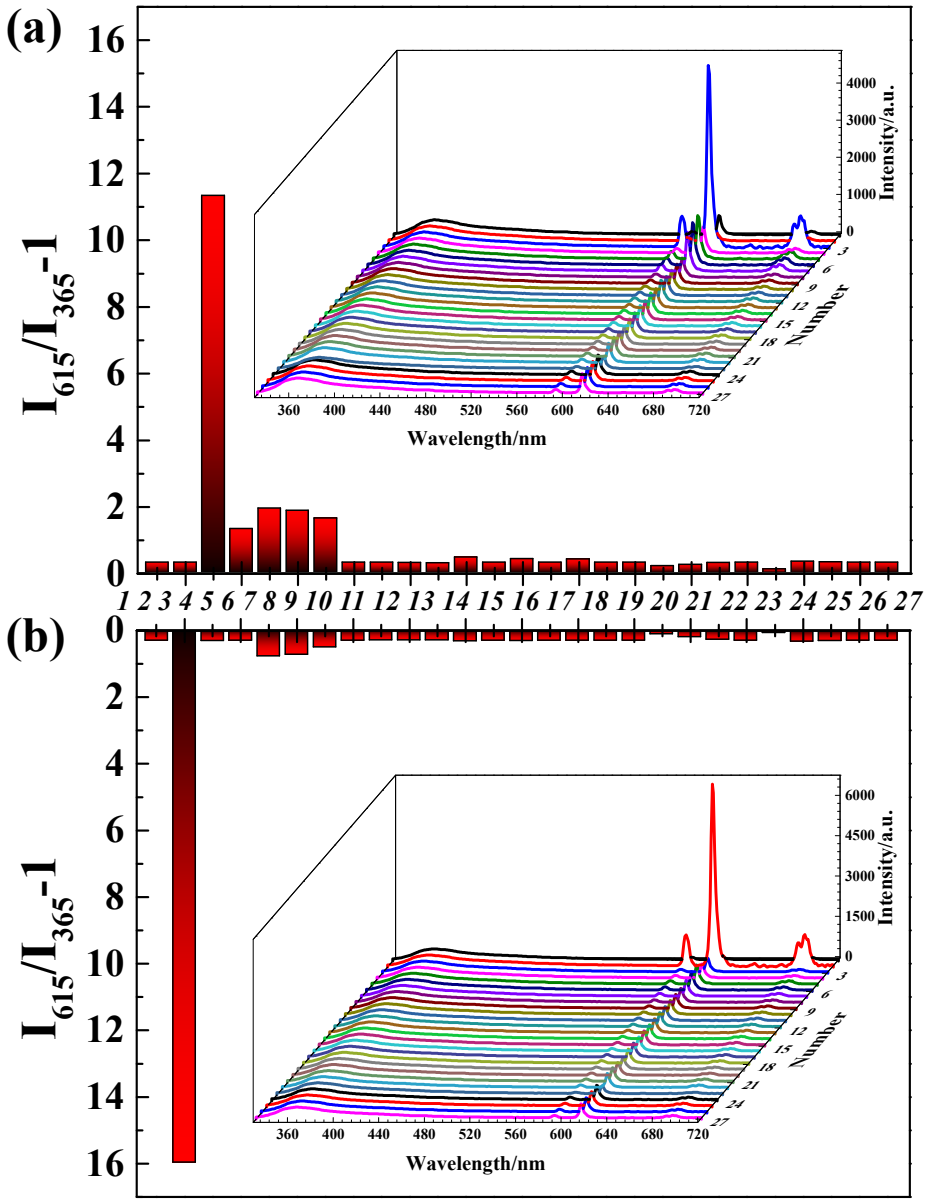

Figure 5. Fluorescence responses of **1a** toward the relevant species (λ_{ex} = 315 nm) (Free(1),

AA(2), H_2S(3), H_2S_2(4) Cys(5), Hcy(6), GSH(7), PO_4^{3-}(8), HPO_4^{2-}(9), CO_3^{2-}(10), HCO_3^-(11), $S_2O_3^{2-}$(12), SO_4^{2-}(13), SO_3^{2-}(14), NO_3^-(15), NO_2^-(16), CH_3COO^-(17), $HCOO^-$(18), I^-(19), Br^-(20), Cl^-(21), F^-(22), Fe^{2+}(23), Zn^{2+}(24), Ca^{2+}(25), K^+(26) and Na^+(27)) in the (a) absence or (b) presence of H_2O_2. Inset: Fluorescence spectra of **1a** towards relevant analytes in the absence or presence of H_2O_2 (The concentration of every analytes is 1 mM while H_2S_2 is 0.1 mM).

In general, there are a variety of chemicals in the human body, so it is necessary to explore whether the proposed sensor can differentiate the target molecule efficiently from other coexisting biological components. For this reason, the competition experiments were also conducted to further investigate the selective ability by checking the fluorescence responses of **1a** toward H_2S or AA in the background of other species. As shown in Figure 6, the dramatically increase of emission intensity at 615 nm induced by H_2S or AA/H_2O_2 is not affected by other coexisting competitive analytes (Figure S19, Supporting Information), indicating the excellent selectivity and high anti-interference ability of **1a**. Furthermore, cyclic performance of **1a** is also investigated. As depicted in Figure S20 (Supporting Information), the fluorescence intensity of **1a** suggested that the addition of H_2O_2 succeeded in realizing the selective detection of AA and H_2S. **1a** still maintains the detection activity of H_2S after several cycles. As a result, the probe **1a** could be used to selective and efficient detection of H_2S and AA, even in the participation of various competitive analytes.

Figure 6. Fluorescence responses of **1a** toward H_2S or AA/H_2O_2 in the existence of other various competitive analytes (λ_{ex} = 315 nm). (H_2S_2(1) Cys(2), Hcy(3), GSH(4), PO_4^{3-}(5), HPO_4^{2-}(6), CO_3^{2-}(7), HCO_3^-(8), $S_2O_3^{2-}$(9), SO_4^{2-}(10), SO_3^{2-}(11), NO_3^-(12), NO_2^-(13), CH_3COO^-(14), $HCOO^-$(15), I^-(16), Br^-(17), Cl^-(18), F^-(19), Fe^{2+}(20), Zn^{2+}(21), Ca^{2+}(22), K^+(23) and Na^+(24)) (The concentration of every analytes is 1 mM while H_2S_2 is 0.1 mM).

Detection of hydrogen sulfide (H_2S) and ascorbic acid (AA) in a wide range

The aforementioned analysis showed that **1a** has excellent detection ability toward single component (H_2S or AA). Then, we introduced the second analyte into the recognition system and explored the molecular recognition ability when H_2S and AA simultaneous existed by fluorescence titration experiment of H_2O_2 (Figure 7 and Figure S21-24, Supporting Information). First of all, the emission of **1a** was attributed to itself and H_2S-treatment before the addition of H_2O_2. As shown in Figure 7a, upon the gradual addition of H_2O_2, the fluorescence intensity dramatically increased with the concentration of H_2O_2 ranging from 0 to 400 μM. Continuing to increase the amount of H_2O_2, the fluorescence intensity tended to decrease until 1000 μM; then remained unchanged. According to the reduction strength of the two analytes (AA > H_2S), the specific process may be identified as follows: AA was first oxidized into DA to sensitize Eu^{3+} ions with the addition of H_2O_2; Then the remaining H_2S was

oxidized to generated sulfur, which has no influence on the fluorescence emission spectra of **1a** (Equation 3).

$$H_2S + 2{\cdot}OH \rightarrow S\downarrow + 2H_2O \quad (3)$$

To further demonstrate the process of the reaction of H_2O_2, AA and H_2S catalyzed by **1a**, UV–Vis spectra of **1a**, H_2S and AA with different concentrations of H_2O_2 were studied. It is obvious that the absorption peak of AA at 263 nm was gradually weakened and disappeared finally with the addition of H_2O_2, which proved that H_2O_2 reacted firstly with AA in solution (Figure S25, Supporting Information). It is also consistent with the slope of the fitted line, showing high switching ratio.

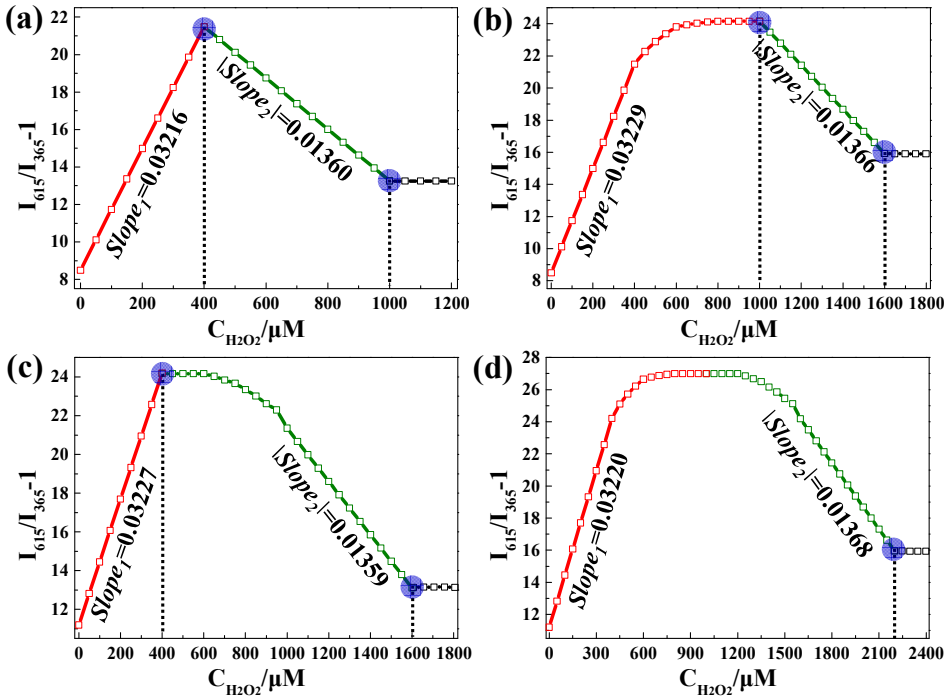

Figure 7. Fluorescence responses of **1a** toward the addition of H_2O_2 in the presence of (a) AA (400 μM) and H_2S (600 μM); (b) AA (1000 μM) and H_2S (600 μM); (c) AA (400 μM) and H_2S (1200 μM); (d) AA (1000 μM) and H_2S (1200 μM)

More importantly, we also studied the fluorescence responses of **1a** toward different concentrations of AA and H_2S, one (or all) of which beyond the detection range. It is worth noting that AA (or H_2S) can be detected quantitatively in a wide range when the concentration of H_2S (or AA) is within the detection range (Figure 7b and 7c), which is rarely reported in the literature. However, when the concentration of H_2S and AA exceed the detection range, only the total concentrations of H_2S and AA

can be obtained (Figure 7d). Similar to the acid-base titration experiment, AA or/and H_2S as substrates as well as **1a** as fluorescent indicator, H_2O_2 was added dropwise to oxidize AA or/and H_2S in turn to realize simultaneous, selective and quantitative detection in a wide range.

Detection of hydrogen sulfide (H_2S) and ascorbic acid (AA) in real samples

To assess the detection efficiency of the newly designed probe in practical application, the detection of H_2S and AA in real samples were explored. Two human serum samples were collected and spiked with different concentrations of H_2S or AA for the detection. As shown in Table 1, all H_2S or AA measured by the newly designed sensor are very close to the total amount of background and spiked H_2S or AA, resulting in satisfying recoveries of 94.7%–104.1%. The calculated relative standard deviation (RSD) was less than 4% based on the five repeated measurements of human serum sample. The satisfactory recovery rate and RSD effectively proved that this method is accurate and reliable in quantitative detection of H_2S or AA in human serum.

Table 1 Determination of H_2S or AA in real human serum samples by standard addition method.

Samples	Concentration of H_2S (μM)			RSD [b] (n=5, %)	Recovery (%)
	Background	Spiked	Found [a] (Mean±SD)		
Human serum-1	8.91	10	18.50 ± 0.32	1.73	97.8
		20	27.79 ± 0.92	3.31	95.8
Human serum-2	14.72	10	25.25 ± 0.59	2.33	102.1
		20	36.14 ± 1.25	3.46	104.1
Samples	Concentration of AA (μM)			RSD [b] (n=5, %)	Recovery (%)
	Background	Spiked	Found [a] (Mean±SD)		
Human serum-1	21.22	20	39.04 ± 0.83	2.13	94.7
		40	58.47 ± 1.40	2.39	95.5
Human serum-2	30.16	20	48.96 ± 1.86	3.80	97.6
		40	71.05 ± 2.22	3.12	101.3

[a] All concentrations were expressed as mean of five measurements ± standard deviation (SD)

[b] The relative standard deviation (RSD) was defined as (SD/mean)×100%.

Molecular logic operation

Inspired by the above observations regarding the fluorescence responses of **1a** toward different analytes (H_2S, AA and H_2O_2), we have experimentally constructed a fluorescence logic system which can perform multiplexed analysis of different

analytes in solution.[51-53] In the logic operation, **1a** served as gate, while different analytes (H_2O_2, AA and H_2S) and fluorescence intensity ratio (I_{615}/I_{365}) were designated as chemical inputs and output, respectively.[54] An input is "on" (*i.e.*, 1) when the analyte was injected, and it is "off" (*i.e.*, 0) when the analyte was not injected. Further, the output was set as 0 (lower) or 1 (higher) by comparison with the prescribed threshold value (I_{615}/I_{365}: 8.0). Subsequently, a parallel logic circuit composed of an AND gate and an INH gate was achieved (Figure 8 and Figure S26, Supporting Information). The first AND gate was constructed by employing H_2O_2 and AA as double inputs since the fluorescence response of AA relies on the injection of H_2O_2. On the other hand, the addition of H_2S to **1a** triggers self-assembly between H_2S and **1a**, showing a clear-cut and significant red fluorescence. But the reductive H_2S could be oxidized by the second input H_2O_2, showing no influence on the fluorescence of **1a**. Therefore, a binary INH logic operation which has turn-on output only in the presence of one particular input could be constructed by employing H_2O_2 and H_2S as double inputs. In other words, the open of the INH gate relies on the introduction of H_2S. There are and only the injection of H_2S can set off turn-on response. Based on the above observations, we have further achieved an combinatorial gate "AND(INH)–OR by combining the AND gate with the INH gate in parallel. The outputs of the AND gate and INH gate were defined as the inputs of the next OR gate. The expected activity of the integrative logic operation "AND(INH)–OR" was confirmed by fluorescence measurements (Figure 8d), accord with the truth table for the logic operation.

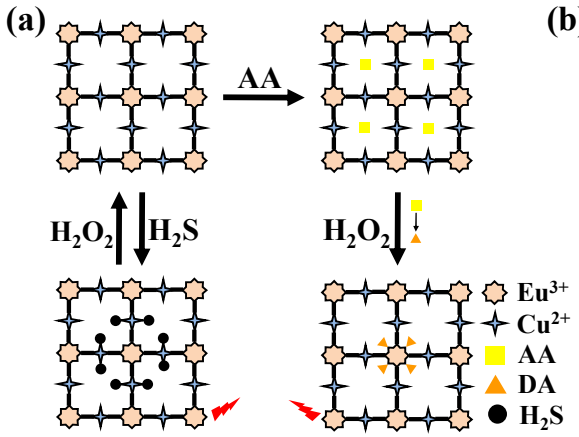

(b)

No.	Inputs			Outputs
	H_2O_2	AA	H_2S	I_{615}/I_{365}
1	0	0	0	0
2	1	0	0	0
3	0	1	0	0
4	0	0	1	1
5	1	1	0	1
6	1	0	1	0
7	0	1	1	1
8	1	1	1	1

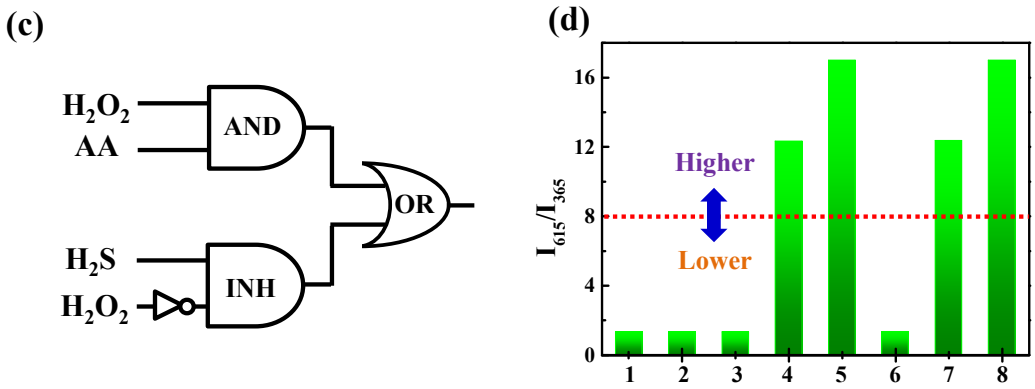

Figure 8. (a) Operational design of the AND(INH)-OR gate, using H_2O_2 (2 mM), AA (1 mM) and H_2S (1 mM) as the three inputs and I_{615}/I_{365} as the output; (b) Truth table of the AND(INH)-OR gate; (c) Electronic equivalent circuitry of the AND(INH)-OR gate; (d) Column diagram of the fluorescence intensity ratio in different states: the red dashed line shows the threshold (I_{615}/I_{365}:8.0).

■ CONCLUSION

In summary, we have successfully reported a novel bimetallic biosensor $[EuCu(pydc)_2(ox)_{0.5}(H_2O)_3 \cdot 1.5H_2O]_{2n}$ (**1**), which provides abundant active sites for highly sensitive detection of AA or H_2S in bio-mimic environment. The excellent hydrolytic stability, recyclability and fluorescence "turn-on" sensing mechanism make it particularly suitable for application in real samples. More importantly, selective and quantitative detection of AA and H_2S in a wide range (H_2S: [130 nM, +∞); AA: [55 nM, +∞)) was realized through the introduction of H_2O_2. To the best of our knowledge, it is the first attempt to directly apply MOFs as a biosensor for the simultaneous detection of H_2S and AA in a wide range, showing high switching ratio. At the same time, **1a** is also found to exhibit excellent peroxidase-like activity and

follow Michaelis–Menten behavior with a lower Michaelis–Menten constant (K_m = 3.0 mM) than horseradish peroxidase (HRP) (K_m = 3.7 mM). Notably, inspired by the fluorescence properties of **1a** toward different analytes (H_2S, AA and H_2O_2), an multilayered gate cascade (AND(INH)–OR) has been achieved to expand the application of **1a** in biological systems. Last but not least, the activated **1a** may help analyze the elusive mechanisms of some biological processes, which far surpass the concept of sensing itself.

■ EXPERIMENTAL SECTION

Synthesis of $[EuCu(pydc)_2(ox)_{0.5}(H_2O)_3 \cdot 1.5H_2O]_{2n}$ (1)

The mixture of $Eu(NO_3)_3 \cdot 6H_2O$ (0.1 mmol, 44.6 mg), $Cu(NO_3)_2 \cdot 3H_2O$ (0.1 mmol, 24.1 mg), H_2pydc (0.2 mmol, 52 mg), and $Na_2C_2O_4$ (0.1 mmol, 13.6 mg) in 10 mL mixed solvent (CH_3CN: H_2O, 1:1) was placed in a Teflon-lined autoclave (25 mL). Then the final mixture was heated at 120 °C for 3 days. After the autoclave was cooled to room temperature at 10 °C·h^{-1}, blue crystal suitable for single crystal X-ray crystallographic analysis was obtained. The mother liquor was decanted, and the crystal was rinsed three times with methanol (10 mL × 3) and dried in air for 2 h. Yield: ≈ 61 %; FT-IR (KBr pellet, cm^{-1}) (Figure S27, Supporting Information) for **1**: 3205 (br, m), 3081 (s), 1656 (s), 1625 (s), 1365 (s), 1272 (s), 1160 (s), 1118 (s), 875 (w), 838 (m), 727 (m), 696 (m), 615 (w), 539 (w), 503 (w), 440 (w). Elemental analysis calculated (%) for $C_{30}H_{18}Cu_2Eu_2N_4O_{29}$: C 27.07, H 1.35, N 4.21; found: C 27.21, H 1.46, N 4.05.

Activation of as-synthesized 1

The fresh sample of **1** was added in 10 mL methanol for solvent exchanged for 12 h. This procedure was repeated three times. Then, the sample was dried under high vacuum at 180 °C for 10 h, obtaining anhydrous activated sample **1a**.

Detection of hydrogen sulfide (H_2S) and ascorbic acid (AA)

For the experiment of sensing H_2S and AA, powder sample of **1a** (3 mg) was added into HEPES buffer (3 mL) (10 mM, pH = 7.4) of AA/H_2O_2 (2 mM/5 mM) and H_2S (2 mM), respectively. The mixtures were subsequently shaken to form suspension for

fluorescent measurement with the excitation at 315 nm.

Enzyme-kinetics analysis of 1a

Steady-state kinetic assay was performed at room temperature. The peroxidase-like activity of **1a** was investigated by adding **1a** (3 mg) into HEPES buffer (10 mM, pH = 7.4) with AA (1 mM), and the total reaction volume is 3 mL. Then different concentrations of H_2O_2 (1 mM, 2 mM, 3 mM, 4 mM, 5 mM, 6 mM, 7 mM, 8 mM, 9 mM and 10 mM) were added, and the emission spectra was recorded with the excitation at 315 nm. According to the linear relationship of the fluorescence intensity and the concentration of reactant, K_m and V_{max} were calculated based on the Michaelis-Menten equation (4):

$$V = V_{max} \times [S]/(K_m+[S]) \quad (4)$$

Where V is the initial velocity, V_{max} is the maximal reaction velocity, [S] is the concentration of substrate and K_m is the Michaelis constant.

Selective detection of hydrogen sulfide (H_2S) and ascorbic acid (AA)

The solutions of various testing species were prepared from AA, H_2S, H_2S_2, Hcy, Cys, GSH, PO_4^{3-}, HPO_4^{2-}, CO_3^{2-}, HCO_3^-, $S_2O_3^{2-}$, SO_4^{2-}, SO_3^{2-}, NO_3^-, NO_2^-, CH_3COO^-, $HCOO^-$, I^-, Br^-, Cl^-, F^-, Fe^{2+}, Zn^{2+}, Ca^{2+}, K^+ and Na^+ in HEPES buffer (10 mM, pH = 7.4) with the total volume of 3 mL (the concentration of every analytes is 1 mM while H_2S_2 is 0.1 mM). Then fresh powder sample of **1a** (3 mg) was added. These mixtures were mixed well and then shaken to form suspension for the first fluorescent measurement. After that, 5 mM H_2O_2 was added and the mixtures were shaken for 5 min for the second fluorescent measurement.

Collections and pretreatments of real sample

Fresh human serum samples were acquired by centrifugation at 5000 rpm for 10 min to remove the proteins and cellular debris from human whole blood samples which were collected from healthy young volunteers treated in the local hospital. Note: 0.2 mM dimethylthiourea (a well-known H_2O_2 scavenger) was added to each serum sample before H_2S detection.

■ ASSOCIATED CONTENT

Supporting Information

X-ray crystallographic files (CIF), Structural Information for MOF **1**, IR spectra, fluorescence spectra, TGA curves, PXRD patterns, and selected bond lengths and angles for MOF **1**. This information is available free of charge *via* the Internet http://pubs.acs.org.

■ AUTHOR INFORMATION

Corresponding Authors

*E−mail: fanruiqing@hit.edu.cn

*E−mail: ylyang@hit.edu.cn

ORCID

Xubin Zheng: 0000-0001-7365-1902

Ruiqing Fan: 0000-0002-5461-9672

Yulin Yang: 0000-0002-2108-662X

Notes

The authors declare no competing financial interest.

■ ACKNOWLEDEGMENTS

This work was supported by National Natural Science Foundation of China (Grant No. 21873025, 21571042 and 51603055). We also like to thank the referees for their constructive comments.

■ REFERENCES

(1) Zhang, D.; Macinkovic, I.; Devarie-Baez, N. O.; Pan, J.; Park, C. M.; Carroll, K. S.; Filipovic, M. R.; Xian, M. Detection of Protein S-Sulfhydration by a Tag-Switch Technique. *Angew. Chem. Int. Ed.* **2014**, *53*, 575-581.

(2) Zheng, Y.; Yu, B.; Ji, K.; Pan, Z.; Chittavong, V.; Wang, B. Esterase-Sensitive Prodrugs with Tunable Release Rates and Direct Generation of Hydrogen Sulfide. *Angew. Chem. Int. Ed.* **2016**, *55*, 4514-4518.

(3) Poole, T. H.; Reisz, J. A.; Zhao, W.; Poole, L. B.; Furdui, C. M.; King, S. B.

Strained Cycloalkynes as New Protein Sulfenic Acid Traps. *J. Am. Chem. Soc.* **2014**, *136*, 6167-6170.

(4) Fukuto, J. M.; Carrington, S. J.; Tantillo, D. J.; Harrison, J. G.; Ignarro, L. J.; Freeman, B. A.; Chen, A.; Wink, D. A. Small Molecule Signaling Agents: The Integrated Chemistry and Biochemistry of Nitrogen Oxides, Oxides of Carbon, Dioxygen, Hydrogen Sulfide, and Their Derived Species. *Chem. Res. Toxicol.* **2012**, *25*, 769-793.

(5) Wang, R. Physiological Implications of Hydrogen Sulfide: a Whiff Exploration that Blossomed. *Physiol. Rev.* **2012**, *92*, 791-896.

(6) Yu, F.; Han, X.; Chen, L. Fluorescent Probes for Hydrogen Sulfide Detection and Bioimaging. *Chem. Commun.* **2014**, *50*, 12234-12249.

(7) Kamoun, P.; Belardinelli, M. C.; Chabli, A.; Lallouchi, K.; Chadefaux-Vekemans, B. Endogenous Hydrogen Sulfide Overproduction in Down Syndrome. *Am. J. Med. Genet. Sect. A.* **2003**, *116A*, 310-311.

(8) Eto, K.; Asada, T.; Arima, K.; Makifuchi, T.; Kimura, H. Brain Hydrogen Sulfide is Severely Decreased in Alzheimer's Disease. *Biochem. Biophys. Res. Commun.* **2002**, *293*, 1485-1488.

(9) Cao, Q.; Zhang, L.; Yang, G.; Xu, C.; Wang, R. Butyrate-Stimulated H_2S Production in Colon Cancer Cells. *Antioxid. Redox Signaling* **2010**, *12*, 1101-1109.

(10) Lin, V. S.; Lippert, A. R.; Chang, C. J. Cell-Trappable Fluorescent Probes for Endogenous Hydrogen Sulfide Signaling and Imaging H_2O_2-Dependent H_2S Production. *Proc. Natl. Acad. Sci. U. S. A.* **2013**, *110*, 7131-7135.

(11) Szabo, C.; Coletta, C.; Chao, C.; Modis, K.; Szczesny, B.; Pa-papetropoulos, A.; Hellmich, M. R. Tumor-Derived Hydrogen Sulfide, Produced by Cystathionine-β-Synthase, Stimulates Bioenergetics, Cell Proliferation, and Angiogenesis in Colon Cancer. *Proc. Natl. Acad. Sci. U. S. A.* **2013**, *110*, 12474-12479.

(12) Smith, M. K.; Mirica, K. A. Self-Organized Frameworks on Textiles (SOFT): Conductive Fabrics for Simultaneous Sensing, Capture, and Filtration of Gases. *J. Am. Chem. Soc.* **2017**, *139*, 16759-16767.

(13) Song, Y.; Xu, M.; Gong, C.; Shen, Y.; Wang, L.; Xie, Y.; Wang, L. Ratiometric Electrochemical Glucose Biosensor Based on GOD/AuNPs/Cu-BTC MOFs/Macroporous Carbon Integrated Electrode. *Sens. Actuators, B* **2018**, *257*, 792-799.

(14) Nam, H.; Kwon, J. E.; Choi, M.-W.; Seo, J.; Shin, S.; Kim, S.; Park, S. Y. Highly Sensitive and Selective Fluorescent Probe for Ascorbic Acid with a Broad Detection Range through Dual-Quenching and Bimodal Action of Nitronyl-Nitroxide. *ACS Sens.* **2016**, *1*, 392-398.

(15) Ren, T. B.; Xu, W.; Zhang, Q. L.; Zhang, X. X.; Wen, S. Y.; Yi, H. B.; Yuan, L.; Zhang, X. B. Enhancing the Anti-Solvatochromic Two-Photon Fluorescence for Cirrhosis Imaging by Forming a Hydrogen-Bond Network. *Angew. Chem. Int. Ed.* **2018**, *57*, 7473-7477.

(16) Liu, T.; Lin, J.; Li, Z.; Lin, L.; Shen, Y.; Zhu, H.; Qian, Y. Imaging of Living Cells and Zebrafish *in vivo* Using a Ratiometric Fluorescent Probe for Hydrogen Sulfide. *The Analyst* **2015**, *140*, 7165-7169.

(17) Yuan, L.; Jin, F.; Zeng, Z.; Liu, C.; Luo, S.; Wu, J. Engineering a FRET Strategy to Achieve a Ratiometric Two-Photon Fluorescence Response with a Large Emission Shift and Its Application to Fluorescence Imaging. *Chem. Sci.* **2015**, *6*, 2360-2365.

(18) Chen, W.; Pacheco, A.; Takano, Y.; Day, J. J.; Hanaoka, K.; Xian, M. A Single Fluorescent Probe to Visualize Hydrogen Sulfide and Hydrogen Polysulfides with Different Fluorescence Signals. *Angew. Chem. Int. Ed.* **2016**, *55*, 9993-9996.

(19) Yassine, O.; Shekhah, O.; Assen, A. H.; Belmabkhout, Y.; Salama, K. N.; Eddaoudi, M. H_2S Sensors: Fumarate-Based fcu-MOF Thin Film Grown on a Capacitive Interdigitated Electrode. *Angew. Chem. Int. Ed.* **2016**, *55*, 15879-15883.

(20) Dong, X.; Su, Y.; Lu, T.; Zhang, L.; Wu, L.; Lv, Y. MOFs-Derived Dodecahedra Porous Co_3O_4 : An Efficient Cataluminescence Sensing Material for H_2S. *Sens. Actuators, B* **2018**, *258*, 349-357.

(21) Tan, H.; Ma, C.; Gao, L.; Li, Q.; Song, Y.; Xu, F.; Wang, T.; Wang, L. Metal-Organic Framework-Derived Copper Nanoparticle@Carbon Nanocomposites as Peroxidase Mimics for Colorimetric Sensing of Ascorbic Acid. *Chem. Eur. J.* **2014**,

20, 16377-16383.

(22) Hao, J.-N.; Yan, B. Determination of Urinary 1-Hydroxypyrene for Biomonitoring of Human Exposure to Polycyclic Aromatic Hydrocarbons Carcinogens by a Lanthanide-functionalized Metal-Organic Framework Sensor. *Adv. Funct. Mater.* **2017**, *27*, 1603856.

(23) Xu, X.-Y.; Yan, B. Intelligent Molecular Searcher from Logic Computing Network Based on Eu(III) Functionalized UMOFs for Environmental Monitoring. *Adv. Funct. Mater.* **2017**, *27*, 1700247.

(24) Lu, L.; Chan, D. S.-H.; Kwong, D. W. J.; He, H.-Z.; Leung, C.-H.; Ma, D.-L. Detection of Nicking Endonuclease Activity Using a G-Quadruplex-Selective Luminescent Switch-on Probe. *Chem. Sci.* **2014**, *5*, 4561-4568.

(25) Vellaisamy, K.; Li, G.; Ko, C.-N.; Zhong, H.-J.; Fatima, S.; Kwan, H.-Y.; Wong, C.-Y.; Kwong, W.-J.; Tan, W.; Leung, C.-H.; Ma, D.-L. Cell Imaging of Dopamine Receptor Using Agonist Labeling Iridium(III) Complex. *Chem. Sci.* **2018**, *9*, 1119-1125.

(26) Hori, Y.; Otomura, N.; Nishida, A.; Nishiura, M.; Umeno, M.; Suetake, I.; Kikuchi, K. Synthetic-Molecule/Protein Hybrid Probe with Fluorogenic Switch for Live-Cell Imaging of DNA Methylation. *J. Am. Chem. Soc.* **2018**, *140*, 1686-1690.

(27) Wang, H.; Feng, Z.; Del Signore, S. J.; Rodal, A. A.; Xu, B. Active Probes for Imaging Membrane Dynamics of Live Cells with High Spatial and Temporal Resolution over Extended Time Scales and Areas. *J. Am. Chem. Soc.* **2018**, *140*, 3505-3509.

(28) Sessoli, R.; Powell, A. K. Strategies Towards Single Molecule Magnets Based on Lanthanide Ions. *Coord. Chem. Rev.* **2009**, *253*, 2328-2341.

(29) Lin, J.; Diefenbach, K.; Silver, M. A.; Dalal, N. S.; Albrecht-Schmitt, T. E. Structure–Property Correlations in the Heterobimetallic 4f/3d Materials $Ln_2M(TeO_3)_2(SO_4)$ (Ln = Y, Nd, Sm, Eu, Gd, Tb, Dy, Ho, Er, Tm, Yb, or Lu; M = Co or Zn). *Cryst. Growth Des.* **2015**, *15*, 4606-4615.

(30) Wang, Y.; Wang, X.-G.; Yuan, B.; Shao, C.-Y.; Chen, Y.-Y.; Zhou, B.-B.; Li, M.-S.; An, X.-M.; Cheng, P.; Zhao, X.-J. Cation-Exchange Porosity Tuning in a

Dynamic 4d–4f–3d Framework for Ni^{II} Ion-Selective Luminescent Probe. *Inorg. Chem.* **2015**, *54*, 4456-4465.

(31) Lustig, W. P.; Mukherjee, S.; Rudd, N. D.; Desai, A. V.; Li, J.; Ghosh, S. K. Metal-Organic Frameworks: Functional Luminescent and Photonic Materials for Sensing Applications. *Chem. Soc. Rev.* **2017**, *46*, 3242-3285.

(32) Xie, Y.-X.; Zhao, W.-N.; Li, G.-C.; Liu, P.-F.; Han, L. A Naphthalenediimide-Based Metal–Organic Framework and Thin Film Exhibiting Photochromic and Electrochromic Properties. *Inorg. Chem.* **2016**, *55*, 549-551.

(33) Zheng, X.; Fan, R.; Song, Y.; Wang, A.; Xing, K.; Du, X.; Wang, P.; Yang, Y. A Highly Sensitive Turn-on Ratiometric Luminescent Probe Based on Postsynthetic Modification of Tb^{3+}@Cu-MOF for H_2S Detection. *J. Mater. Chem. C* **2017**, *5*, 9943-9951.

(34) Barry, D. E.; Caffrey, D. F.; Gunnlaugsson, T. Lanthanide-Directed Synthesis of Luminescent Self-Assembly Supramolecular Structures and Mechanically Bonded Systems from Acyclic Coordinating Organic Ligands. *Chem. Soc. Rev.* **2016**, *45*, 3244-3274.

(35) Yi, F.-Y.; Chen, D.; Wu, M.-K.; Han, L.; Jiang, H.-L. Chemical Sensors Based on Metal-Organic Frameworks. *ChemPlusChem* **2016**, *81*, 675-690.

(36) Yan, B. Lanthanide-Functionalized Metal-Organic Framework Hybrid Systems To Create Multiple Luminescent Centers for Chemical Sensing. *Acc. Chem. Res.* **2017**, *50*, 2789-2798.

(37) Yang, L.; Powell, D. R.; Houser, R. P. Structural Variation in Copper(I) Complexes with Pyridylmethylamide Ligands: Structural Analysis with a New Four-Coordinate Geometry Index, τ_4. *Dalton Trans.* **2007**, *9*, 955-964.

(38) Zhang, X.; Hu, Q.; Xia, T.; Zhang, J.; Yang, Y.; Cui, Y.; Chen, B.; Qian, G. Turn-on and Ratiometric Luminescent Sensing of Hydrogen Sulfide Based on Metal-Organic Frameworks. *ACS Appl. Mater. Interfaces* **2016**, *8*, 32259-32265.

(39) Liu, B.; Chen, Y. Responsive Lanthanide Coordination Polymer for Hydrogen Sulfide. *Anal. Chem.* **2013**, *85*, 11020-11025.

(40) Aulsebrook, M. L.; Biswas, S.; Leaver, F. M.; Grace, M. R.; Graham, B.; Barrios,

A. M.; Tuck, K. L. A Luminogenic Lanthanide-based Probe for the Highly Selective Detection of Nanomolar Sulfide Levels in Aqueous Samples. *Chem. Commun.* **2017**, *53*, 4911-4914.

(41) He, J.; Huang, J.; He, Y.; Cao, P.; Zeller, M.; Hunter, A. D.; Xu, Z. A Boiling-Water-Stable, Tunable White-Emitting Metal-Organic Framework from Soft-Imprint Synthesis. *Chem. Eur. J.* **2016**, *22*, 1597-1601.

(42) Qi, Z.; Wang, L.; You, Q.; Chen, Y. PA-Tb-Cu MOF as Luminescent Nanoenzyme for Catalytic Assay of Hydrogen Peroxide. *Biosens. Bioelectron.* **2017**, *96*, 227-232.

(43) Dutta, A. K.; Das, S.; Samanta, S.; Samanta, P. K.; Adhikary, B.; Biswas, P. CuS Nanoparticles as a Mimic Peroxidase for Colorimetric Estimation of Human Blood Glucose Level. *Talanta* **2013**, *107*, 361-367.

(44) Gao, L.; Zhuang, J.; Nie, L.; Zhang, J.; Zhang, Y.; Gu, N.; Wang, T.; Feng, J.; Yang, D.; Perrett, S.; Yan, X. Intrinsic Peroxidase-like Activity of Ferromagnetic Nanoparticles. *Nat. Nanotechnol.* **2007**, *2*, 577-583.

(45) Ai, L.; Li, L.; Zhang, C.; Fu, J.; Jiang, J. MIL-53(Fe): a Metal-Organic Framework with Intrinsic Peroxidase-like Catalytic Activity for Colorimetric Biosensing. *Chem. Eur. J.* **2013**, *19*, 15105-15108.

(46) Dong, Y. L.; Zhang, H. G.; Rahman, Z. U.; Su, L.; Chen, X. J.; Hu, J.; Chen, X. G. Graphene Oxide-Fe_3O_4 Magnetic Nanocomposites with Peroxidase-like Activity for Colorimetric Detection of Glucose. *Nanoscale* **2012**, *4*, 3969-3976.

(47) Yue, D.; Zhao, D.; Zhang, J.; Zhang, L.; Jiang, K.; Zhang, X.; Cui, Y.; Yang, Y.; Chen, B.; Qian, G. A Luminescent Cerium Metal-Organic Framework for the Turn-on Sensing of Ascorbic Acid. *Chem. Commun.* **2017**, *53*, 11221-11224.

(48) Gong, X.; Li, Z.; Hu, Q.; Zhou, R.; Shuang, S.; Dong, C. N,S,P Co-Doped Carbon Nanodot Fabricated from Waste Microorganism and Its Application for Label-Free Recognition of Manganese(VII) and *L*-Ascorbic Acid and AND Logic Gate Operation. *ACS Appl. Mater. Interfaces* **2017**, *9*, 38761-38772.

(49) Guo, C.; Jin, Q.; Wang, Y.; Ding, B.; Li, Y.; Huo, J.; Zhao, X. Developing a Unique Metal-Organic Framework-$\{[Cd(abtz)_2(NCS)]\cdot(ClO_4^-)\}_n$ (abtz =

1-(4-aminobenzyl)-1,2,4-triazole) as Fluorescent Probe for Highly Selective and Sensitive Detection of Ascorbic Acid in Biological Liquid. *Sens. Actuators, B* **2016**, *234*, 184-191.

(50) Wang, L.; Gong, C.; Shen, Y.; Ye, W.; Xu, M.; Song, Y. A Novel Ratiometric Electrochemical Biosensor for Sensitive Detection of Ascorbic Acid. *Sens. Actuators, B* **2017**, *242*, 625-631.

(51) Hafiz, M. A.; Kosuru, L.; Younis, M. I. Microelectromechanical Reprogrammable Logic Device. *Nat. Commun.* **2016**, *7*, 11137.

(52) Liu, H.; Wang, J.; Song, S.; Fan, C.; Gothelf, K. V. A DNA-Based System for Selecting and Displaying the Combined Result of Two input Variables. *Nat. Commun.* **2015**, *6*, 10089.

(53) Qian, L.; Winfree, E.; Bruck, J. Neural Network Computation with DNA Strand Displacement Cascades. *Nature* **2011**, *475*, 368-372.

(54) Pu, F.; Ju, E.; Ren, J.; Qu, X. Multiconfigurable Logic Gates Based on Fluorescence Switching in Adaptive Coordination Polymer Nanoparticles. *Adv. Mater.* **2014**, *26*, 1111-1117.

Table of Contents Graphic